

Increased Voltage in CdSe Solar Cells by Mitigation of Charge Carrier Trapping Due to Se Vacancies

Darius Kuciauskas,* Taylor Hill, James R. Sites, Sachit Grover, Yijun Tong, and Scott T. Dunham

Cadmium selenide (CdSe), with a 1.7 eV bandgap, is a promising high-bandgap semiconductor for tandem solar cells, yet device efficiencies are hindered by rapid minority carrier recombination. Here, polycrystalline CdSe solar cells are investigated using radiative emission spectroscopy, time-resolved photoluminescence, and density functional theory, revealing fast (sub-nanosecond) minority carrier trapping by selenium vacancy-related defect states with densities of $(5\text{--}50) \times 10^{17} \text{ cm}^{-3}$, limiting carrier mobility and increasing recombination. By reducing absorber thickness to $\approx 0.5 \mu\text{m}$, trapping effects are mitigated, achieving a record open-circuit voltage of 917 mV, a 165 mV improvement over prior reports. These findings clarify the role of Se vacancies in limiting CdSe solar cell performance and provide insights applicable to CdSe and CdSeTe thin-film photovoltaics. This work advances understanding of defect-mediated losses in II–VI semiconductors and suggests pathways for improving solar cell performance through defect control.

especially for the larger bandgaps where their absorber structure is more complex.^[3] For II–VI semiconductors, CdSe has near-ideal bandgap $E_g = 1.7 \text{ eV}$ for the top junction in a tandem, but CdSe solar-cell performance continues to be relatively poor.^[4–8]

In addition to having a high bandgap junction for tandem cells, CdSe is a model system for understanding defects in II–VI semiconductors. Since 2014,^[9] a ternary $\text{CdSe}_x\text{Te}_{1-x}$ absorber has become standard in “CdTe” thin-film solar cells, which have reached 50 GW_{pp} (peak power) cumulative installations and in 2024 accounted for $\approx 30\%$ of all PV installations in the US.^[10] However, $\text{CdSe}_x\text{Te}_{1-x}$ solar-cell voltage V_{OC} is only $\approx 82\%$ of the detailed-balance limit and is the primary limitation on

power conversion efficiency.^[11] We have recently shown that $\text{CdSe}_x\text{Te}_{1-x}$ electronic defects and their impacts are unusually complex, including charge carrier traps that reduce hole mobility^[12] and near-bandgap band tail states that limit radiative voltage.^[13] Understanding defects in CdSe might help mitigate defects in ternary $\text{CdSe}_x\text{Te}_{1-x}$ to improve single-junction thin film PV. Here we show that some electronic defects (carrier traps) in CdSe are surprisingly similar to those in $\text{CdSe}_x\text{Te}_{1-x}$, which suggests their common origin. At the same time, band tails are significantly smaller in CdSe than in $\text{CdSe}_x\text{Te}_{1-x}$, which indicates different compensation mechanisms in binary II–VI semiconductors and their ternary alloys.

1. Introduction

Single-junction photovoltaic (PV) solar cells have reached 27–28% power conversion efficiencies (GaAs 28.3%, Si 27.3%, perovskites 27%),^[1] and further advances will likely require tandem or multijunction device architectures. Such efforts have primarily been applied to crystalline III–V semiconductors and to polycrystalline hybrid perovskites.^[2] However, III–V solar cells are far from required cost targets for terrestrial applications, and perovskite solar cells have stability/degradation limitations,

D. Kuciauskas
Chemistry and Nanoscience Center
National Renewable Energy Laboratory
Golden, CO 80401, USA
E-mail: Darius.Kuciauskas@nrel.gov

T. Hill, J. R. Sites
Department of Physics
Colorado State University
Fort Collins, CO 80523, USA

T. Hill, S. Grover
California Technology Center
First Solar, Santa Clara, CA 95050, USA

Y. Tong, S. T. Dunham
Department of Electrical and Computer Engineering
University of Washington
Seattle, WA 98195-2500, USA

The ORCID identification number(s) for the author(s) of this article can be found under <https://doi.org/10.1002/admt.202501967>

DOI: 10.1002/admt.202501967

2. Results and Discussion

2.1. Device Results

We report CdSe devices here with record V_{OC} and discuss the factors which limit their device performance. Solar cell fabrication is described in the Experimental Section. Their device structure (illustrated in **Figure 1a**) consists of a glass/TCO/CdSe/PTAA/MoO₃/Au stack. The development of this substrate device stack, and specifically the optimization of the transparent hole-contact layers (PTAA/MoO₃/Au), was described in a conference publication where $V_{OC} = 752 \text{ mV}$ was presented for absorbers with a thickness of $\approx 1.2 \mu\text{m}$.^[6] To mitigate charge carrier trapping (see Sections 2.2–2.5), we reduced the polycrystalline absorber thickness to $\approx 0.5 \mu\text{m}$. Current–voltage

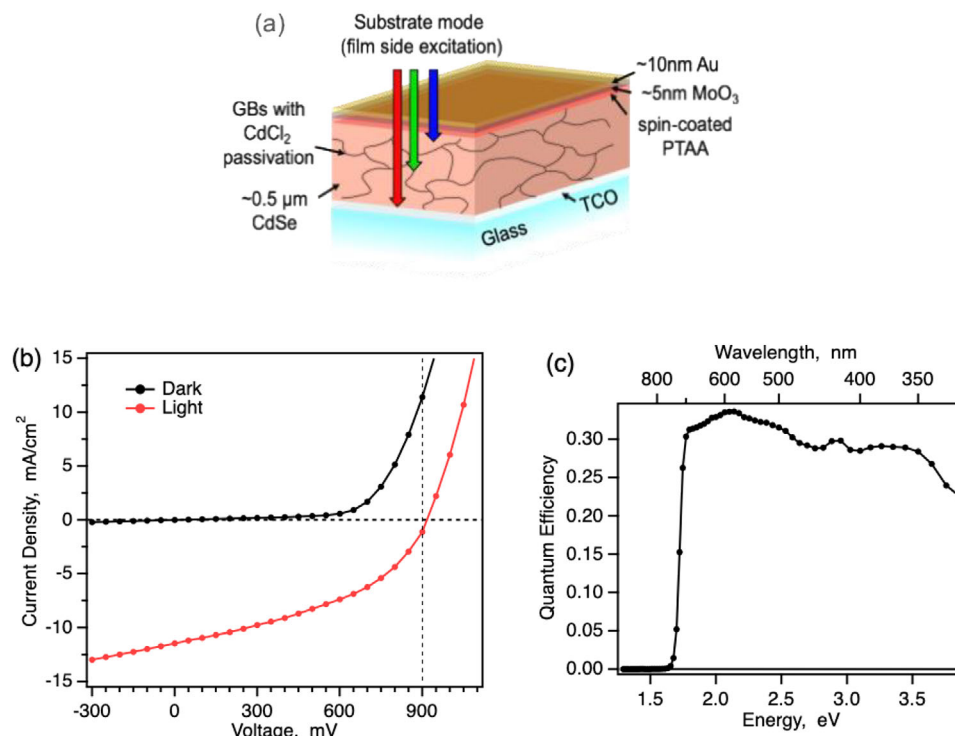


Figure 1. a) Illustration of the device configuration used in this study. TCO is transparent conductive oxide ($\text{SnO}_2:\text{F}$), PTAA is poly(triaryl) amine, GBs are grain boundaries. Dark and light J - V curves b) and EQE spectrum c) for device with a thin ($0.5 \mu\text{m}$) CdSe absorber.

(J - V) and external quantum efficiency (EQE) characteristics for thin absorber devices are shown in Figure 1b,c. Comparing devices with 1.2 vs. $0.5 \mu\text{m}$ absorbers, V_{OC} increased from 752 to 917 mV, short-circuit current J_{SC} was approximately the same, 11.5 mA cm^{-2} , and fill factor FF decreased from 51% to 42.5%.^[6] Power conversion efficiency increased to 4.5% for $0.5 \mu\text{m}$ absorber devices. These results represent a V_{OC} increase of 165 mV from our initial results^[6] and 331 mV from recent publication,^[4] indicating that carrier trapping is a significant loss mechanism in polycrystalline CdSe solar cells. Additional device analysis (V_{OC} , J_{SC} , and fill factor FF) for solar cells where CdSe absorber thickness was varied is presented in Figure S1 (Supporting Information).^[14] As shown in this data, voltage is decreasing with thickness, which indicates increased losses due to trapping. Next, we have applied spectroscopic analysis and density functional theory calculations to help identify electronic defects that can cause charge carrier trapping.

2.2. Emission Spectra

As described in Section 2.1, two film thicknesses were studied, which we label S1 for $1.2 \mu\text{m}$ thick polycrystalline CdSe films on glass/TCO substrates and S2 for $0.5 \mu\text{m}$ films. Figure 2 shows radiative emission spectra at 298 K and at low temperature. The photoluminescence quantum yields (PLQY) at 1-Sun equivalent excitation, PLQY = 2×10^{-4} for S1 and PLQY = 5×10^{-5} for S2, are comparable to polycrystalline solar cells.^[15] For example, for $V_{\text{OC}} = 845 \text{ mV}$ Cu-doped CdSeTe solar cells PLQY = 3×10^{-4} ,^[16] for As-doped $x = 0, 0.2,$ and $0.4 \text{ CdSe}_x\text{Te}_{1-x}$ heterostructures PLQY

= $(0.02-1) \times 10^{-4}$,^[12] and for large-grain Al_2O_3 -passivated undoped $\text{CdSe}_{0.2}\text{Te}_{0.8}$ heterostructures PLQY = 2×10^{-3} ,^[17] which is the highest-reported PLQY for bandgap emission in polycrystalline II-VI semiconductors.

Absorptance spectra calculated from PL using the Generalized Planck's Law are shown in the inset of Figure 2a. The bandgap calculated from the absorptance spectra (using the derivative method)^[18] is $E_g = 1.71 \text{ eV}$. The Stokes shift between absorption and emission is $\approx 10 \text{ meV}$, the same as for crystalline semiconductors, indicating good electronic quality of CdSe absorbers fabricated by vapor transport deposition (VTD). As shown in the inset of Figure 2a, Urbach energies are $E_u = 11.5 \pm 0.1 \text{ meV}$ (S1) and $15.8 \pm 0.1 \text{ meV}$ (S2). The thermal (phonon-limited) E_u at 298 K is 8–9 meV, and the increase of E_u above these values indicates electronic disorder, which can be complex in polycrystalline semiconductors.^[19] The E_u values for our samples, however, are among the lowest-reported for polycrystalline absorbers (e.g., $\approx 13 \text{ meV}$ for hybrid perovskites in the highest-efficiency solar cells^[20] and $\geq 17 \text{ meV}$ for the higher- E_g hybrid perovskites,^[3] $\geq 15 \text{ meV}$ for $\text{Cu}(\text{In,Ga})\text{Se}_2$,^[19] and $\geq 20 \text{ meV}$ for CdSeTe^{13}). Low electronic disorder is further indicated by the 4 K PL emission spectra (Figure 2b), where exciton emission is observed. Two sharp lines in the exciton emission spectral range (1.805–1.795 eV, inset in Figure 2b) have been attributed to bound and free excitons, and broader emission above 1.6 eV to phonon replicas.^[21] Exciton PL at 4 K also identifies wurtzite CdSe phase, as exciton PL would be different in zincblende CdSe.^[22] The low-temperature PL spectrum for S2 is shown in Figure S2 (Supporting Information). This sample has larger exciton peak broadening due to larger electronic disorder in the thinner film.

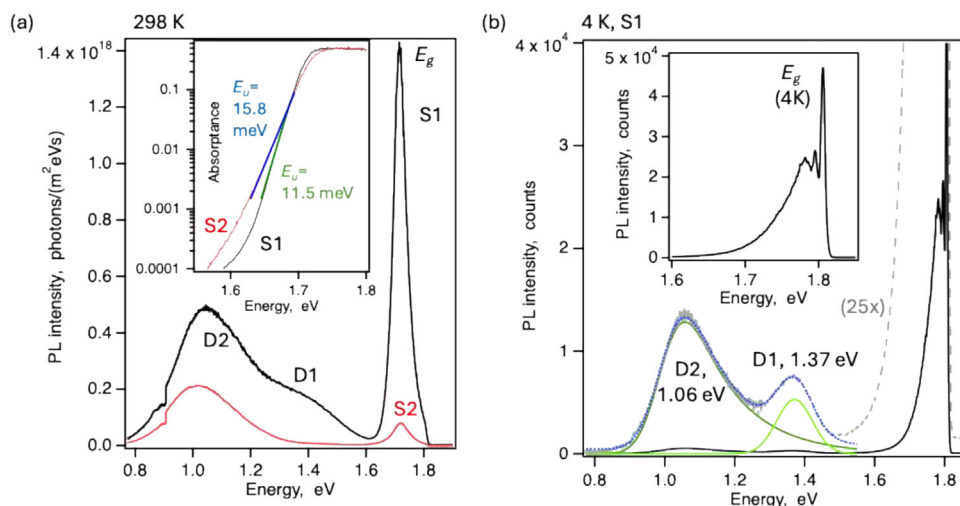


Figure 2. a) Absolute PL emission spectra for S1 (black) and S2 (red) at 298 K. Inset shows absorbance spectra calculated from PL and fits to determine Urbach energies E_U . b) PL emission at 4 K for S1, where D1 and D2 emission spectral region is multiplied by 25× to more clearly show defect emission. The inset shows high energy (exciton) region.

In contrast with most high-efficiency PV semiconductors, strong sub-bandgap defect PL emissions are observed in our CdSe samples. The full width at half magnitude (FWHM) for defect D2 remains approximately the same (258 meV/213 meV at 298 K/4 K), while defect D1 emission is narrower at the low temperature (366 meV/119 meV at 298 K/4 K), strongly suggesting that D2 is a midgap state and that D1 is a shallower defect.

Defects D1 and D2 are well known in CdSe spectroscopy. E.g., Kindleysides and Woods identified similar defect states in photoconductivity and PL spectra of CdSe single crystals, where D1 was photosensitive (in equilibrium with the conduction or valence bands).^[23] Ermolovich and Milenin analyzed D1 and D2 PL emission in single crystal CdSe and in polycrystalline CdSe_xTe_{1-x}.^[24] Brasil et al. constructed configuration energy diagrams and attributed these spectra to V_{Se} (D1) and O_{Se} (D2).^[25] D1 emission persists in CdSe grown by MBE (though the spectral range for D2 was not investigated)^[26] and in thermally evaporated films used to fabricate solar cells.^[5] By using time-resolved measurements,

in Section 2.4 we show that defects D1 and D2 are carrier traps that impact device performance. This aspect was not identified in earlier studies of CdSe semiconductors or solar cells.

Figure 3a shows the temperature dependence for D1 and D2 emission for S1. (The corresponding data for S2 is shown in **Figure S3**, Supporting Information). D1 emission is more complex. Between 4 and 100 K, the D1 PL amplitude increases (≈2.5 times), and then above 100 K it is thermally quenched with an activation energy of $E_A = 130 \pm 15$ meV (fit is shown in **Figure 3b**). These observations are similar to those made by Brasil et al. (maximum of D1 emission was at 1.35 eV and $E_A = 170$ meV), where D1 was assigned to V_{Se}.^[24] First principles studies also considered V_{Se} in CdSe and CdSe_{0.94}Te_{0.04} and estimated density of such defects $>10^{16}$ cm⁻³ when growth temperature was 1100 K.^[7] To verify the D1 assignment, we conducted additional DFT calculations as described in Section 2.3, with particular attention to optical properties, which were not considered in previous first-principle analysis.^[7]

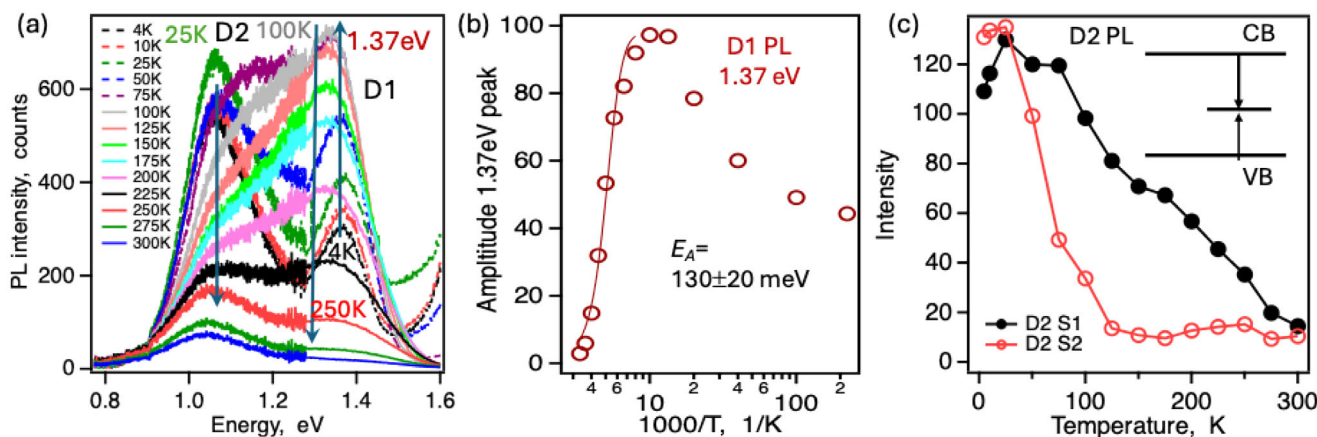


Figure 3. Defect D1 and D2 PL emission. a) Temperature-dependence of defect emission bands for S1. b) Analysis of D1 emission in graph (a) to determine activation energy E_A . c) D2 emission temperature dependence for S1 and S2.

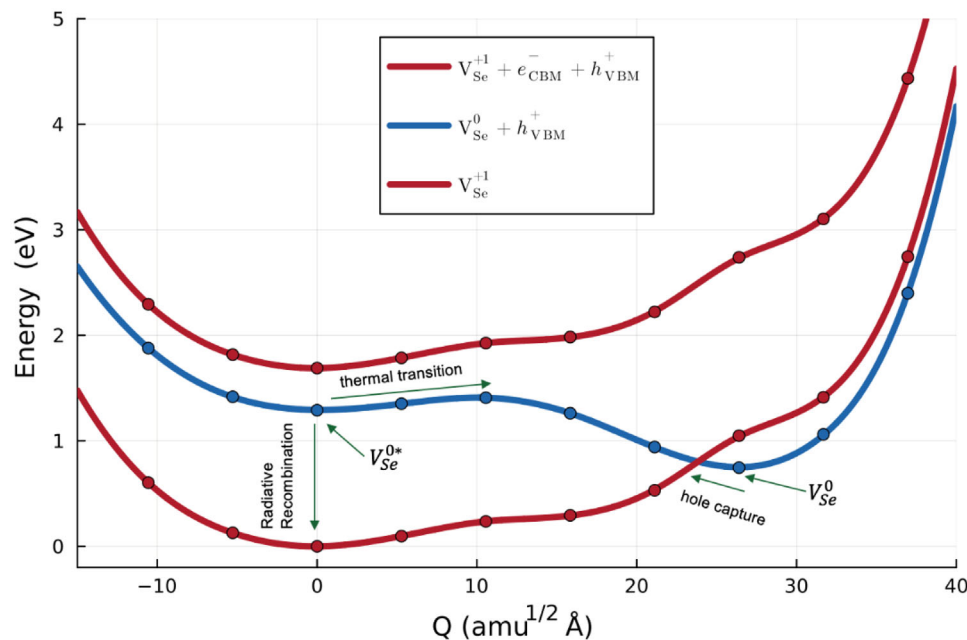


Figure 4. Calculated configuration coordinate diagram (CCD) between V_{Se}^0 and V_{Se}^{+1} . Q represents the distance in configuration space projected linearly between the ground state structures of +1 ($Q = 0$) and neutral ($Q = 27$) Se vacancies. Arrows show the key processes manifested in PL and solar cell behavior as described in the text. The metastable neutral vacancy V_{Se}^{0*} , which has nearly the same structure as the +1 (and +2) ground states, plays a key role in the optoelectronic response.

Defect D2 follows a simpler emission quenching model, Figure 3c.^[23,24] Two activation energies are required to fit D2 quenching. The first sample-dependent activation energy is 22–40 meV, and the second activation energy is >0.3 eV, amplitude of which is higher for S2. Using a temperature range up to 550 K allowed determination of 0.8 eV activation energy for D2,^[24] making it a near-midgap defect. Time-resolved data (Section 2.4) shows that carriers can be detrapped from D1 but not from D2, in agreement with D2 assignment as a deep trap. Assignment of D2 emission to O_{Se} was suggested,^[24] which is possible in our samples where CdSe film was grown on oxide substrate and then annealed to facilitate grain growth.^[6] The difference in D2 PL band thermal quenching behavior between S1 and S2 (Figure 3c) is in agreement with a D2 attribution to extrinsic defects.

2.3. Density Functional Theory (DFT) Calculations

Selenium vacancies are dominant defects in CdSe^[7,27] and have been suggested to account for some of the observed optoelectronic behavior.^[24] To understand their impact in more detail, DFT calculations were performed as described in the Computational Methods section below. Three charge states of Se vacancies were calculated: neutral, +1 and +2. The thermodynamic transition level (above VBM) is 1.6352 eV for (+2/+1) and 0.7463 eV for (+1/0), which indicates negative- U behavior. The configuration coordinate diagram (CCD) between V_{Se}^0 and V_{Se}^{+1} is shown in Figure 4. The V_{Se}^{+2} and V_{Se}^{+1} atomic structures are nearly identical and the associated charge distributions indicate that V_{Se}^{+1} is essentially V_{Se}^{+2} with a delocalized bound electron. This is consistent with the +2/+1 ionization level location just below

conduction band minimum. As seen in Figure 4, V_{Se}^0 shows a metastable state (noted as V_{Se}^{0*}) which shares the same structure as the ground state of $V_{\text{Se}}^{+1/+2}$ and has a second delocalized electron.

Based on the calculated ionization levels, the majority of selenium vacancies in undoped CdSe is in the stable V_{Se}^0 structure under equilibrium conditions. During illumination, fast hole trapping induces a transient boost in the concentration of V_{Se}^{+1} , which can (1) transition into V_{Se}^{+2} by emitting an electron, (2) transition into V_{Se}^{0*} by capturing an electron, or (3) detrapp the captured hole and relax back to V_{Se}^0 . Process (3) is slow due to large barrier and thus can generally be ignored. Process (1) is reversible and relatively rapid, allowing equilibration of the +1/+2 vacancy populations. Process (2) populates the metastable V_{Se}^{0*} state. There are two primary paths for relaxation of this metastable state: 1) photon emission via recombination of free hole with bound electron and 2) transformation to stable neutral V_{Se}^0 via structural deformation. The V_{Se}^{0*} radiative recombination pathway emits photons with energy calculated to be ≈ 1.3 eV, closely matching the experimental D1 PL value of ≈ 1.35 eV. The structural transformation from V_{Se}^{0*} to stable V_{Se}^0 , which involves symmetric contraction of the surrounding Cd atoms toward the vacant site, requires overcoming an energy barrier and thus is temperature dependent. As temperature is increased, the thermal transition from metastable V_{Se}^{0*} to stable V_{Se}^0 will depopulate V_{Se}^{0*} and thus cause the defect PL to decrease. The ≈ 150 meV barrier is likely to be the cause of D1 PL quenching above 100 K and matches well with the experimentally observed activation energy of 130 meV (this work) and 170 meV (Brasil et al.^[24]).

The asymmetry between fast hole trapping from V_{Se}^0 to V_{Se}^{+1} and slow hole detrapping from V_{Se}^{+1} to V_{Se}^0 is also consistent

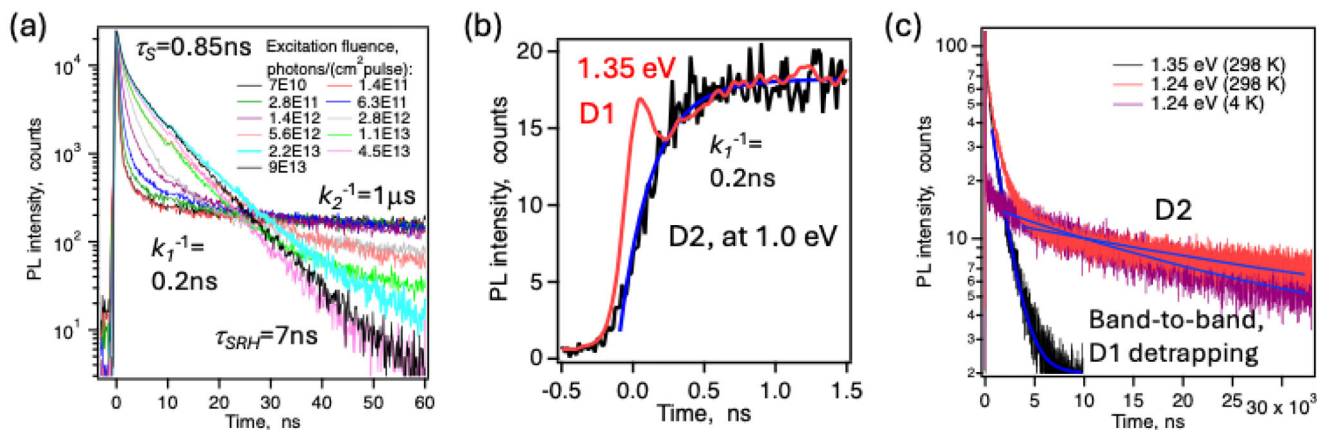


Figure 5. Summary of carrier dynamics. a) Injection-dependent bandgap PL emission. Excitation fluences are indicated in the legend. b) Dynamics of photocarrier capture to D1 (red, measured at 1.35 eV) and D2 (black, measured at 1.0 eV) states. Blue line indicates fit with $k_1^{-1} = 0.2$ ns. c) Longer-time dynamics for D1 (black measured at 1.35 eV, solid line is a fit with $k_2^{-1} = 1.0$ μ s) and D1/D2 (measured at 1.24 eV, D2 lifetime 32 μ s at 298 K and 19 μ s at 4 K).

with experimental results, as discussed below. Under illumination, most of the generated holes are trapped via formation of positively-charged Se vacancies, which slowly decay via electron capture by way of the neutral metastable state.

2.4. Carrier Dynamics

Time-resolved photoluminescence (TRPL) data is shown in **Figure 5**. At low injection, PL from near the bandgap is quenched with $k_1^{-1} = 0.2$ ns (Figure 5a) and defect D1 and D2 emission increases with the same rate (Figure 5b), which is direct evidence of carrier capture to D1 and D2 states. When injection is increased, amplitude of the fast decay component for the bandgap emission becomes smaller until bandgap TRPL approaches a single exponential. This is attributed to saturation of D1 and D2 traps with photoinjected carriers. Using excitation fluence of this saturation (6×10^{13} photons cm^{-2} pulse $^{-1}$), we estimate trap density [D1] + [D2] = (5–50) $\times 10^{17}$ cm^{-3} ; lower if carriers are equilibrated over the film thickness and higher if confined to the initial absorption depth.

TRPL lifetimes τ_{TRPL} measured when traps are saturated indicate Shockley-Read-Hall (SRH) recombination lifetime, $\tau_{\text{SRH, film}} = 7$ ns. Similar $\tau_{\text{TRPL}} \approx \tau_{\text{SRH, device}} = 4$ ns was measured using high-excitation-fluence TRPL on a full device stack.^[6] The difference between $\tau_{\text{SRH, film}} = 7$ ns and $\tau_{\text{SRH, device}} = 4$ ns can indicate additional recombination at the device interfaces.^[27] Lifetime τ_{SRH} establishes the minority carrier density and thus the minority carrier quasi-Fermi level (qFL). Between absorber film and full device stack minority carrier qFL would change by

$$\frac{k_B T}{e} \ln \left(\frac{\tau_{\text{SRH, device}}}{\tau_{\text{SRH, film}}} \right) \quad (1)$$

where k_B is Boltzmann's constant, T is temperature, and e is elementary charge.^[28] This approximation yields an additional 26 mV $\times \ln(4\text{ns}/7\text{ns}) \approx -15$ mV hole-contact interface recombination loss. Interface losses are similar in highly efficient solar

cells,^[27] suggesting that hole contact optimization procedure reported earlier was successful.^[6] Recombination at the electron contact is also seen here to not be significant. As shown in Figure S4 (Supporting Information), using the initial part of bandgap TRPL decay, it is possible to estimate the upper limit for the interface recombination velocity at the electron contact, $S_{\text{electron}} \leq 2 \times 10^4$ cm s^{-1} .

Carrier lifetime of 7 ns is low in comparison to highly efficient solar cells, but appears to be the best-reported for CdSe, resulting in increased voltages in our study. Xue et al. reported that carrier lifetime (measured in films) increased from 0.53 to 1.43 ns by alloying CdSe to form CdSe_{0.96}Te_{0.04}.^[7] Li et al reported bi-exponential TRPL decay with $\tau_1 = 0.28$ ns (which could indicate trapping) and $\tau_2 = 1.34$ ns.^[4] Bastola et al. reported complex TRPL decay with a tail lifetime of 100 ns and higher.^[5] This dynamics was likely due to detrapping from the D1 state, as shown in the low-injection data in Figure 5a and discussed next.

We analyze defect state dynamics from data in Figure 5c. Lifetime for D1 emission and bandgap emission tail lifetime at low injection of $k_2^{-1} \approx 1.0 \pm 0.1$ μ s is attributed to hole detrapping from D1. Trapping/detrapping to/from the D1 state helps understand charge transport in CdSe solar cells. Because minority carrier capture to defects is very fast ($k_1^{-1} = 0.2$ ns), carriers cannot be collected by electron and hole contacts immediately after photogeneration. Instead, trapping/detrapping repeats many times, resulting in charge transport than can be described by low mobility.^[12] In CdSeTe solar cells, simulations of transport limited by hole traps were reported, where it was shown that such transport leads to reduction in voltage and fill factor.^[12,13] When trapping is reduced, mobility increases more than an order of magnitude.^[29] We analyze transport in Section 2.5.

Finally, photocarrier lifetimes in the deeper D2 state are 32 ± 3 μ s at 298 K and 19 ± 2 μ s at 4 K, Figure 5c. Such very long and near-temperature-independent lifetimes are typical for deep states, and carriers in such deep trap states do not contribute to photocurrent.

2.5. Trapping Impact on CdSe Solar Cells

Solar cell voltage V_{OC} is often evaluated starting with thermodynamic properties of radiative voltage V_{OC}^{rad} and implied voltage iV_{OC} , which are related as:^[17]

$$iV_{OC} = V_{OC}^{rad} + \frac{k_B T}{e} \ln(PLQY) \quad (2)$$

The radiative voltage V_{OC}^{rad} establishes voltage entitlement, and implied voltage iV_{OC} is reduced due to non-radiative recombination, which is quantified by PLQY. The bandgap for our samples is $E_g = 1.71$ eV, and the detailed-balance voltage for this bandgap is $V_{OC}^{SQ} = 1.41$ V.^[30] When band tails increase to $E_u = 10$ – 15 meV, corresponding to values for our samples, voltage entitlement V_{OC}^{SQ} is reduced by 10–30 mV,^[31] to $V_{OC}^{rad} = 1.38$ – 1.40 V. Since $PLQY = 2 \times 10^{-4}$ for S1 and 5×10^{-5} for S2, Figure 2a, $iV_{OC} = 1.17$ – 1.18 V (S1) and $iV_{OC} = 1.13$ – 1.14 V (S2). Such iV_{OC} estimates can be verified by fitting emission spectra.^[32] As shown in Figure S5 (Supporting Information), spectral analysis suggests $iV_{OC} = 1.14 \pm 0.02$ V for S1 in our data. A similar $iV_{OC} = 1.1$ V estimate for CdSe was reported.^[4]

Relating absorptance and radiative efficiency to iV_{OC} (also called quasi-Fermi level splitting, qFLS) as described by Equation (2) and other thermodynamic models^[17–19,29,30] assumes (near) perfect charge carrier transport, which can be expressed as “infinite mobility” and/or charge carrier diffusion length exceeding absorber thickness.^[33] Measurement of radiative emission alone, such as in Figure 2, does not verify this assumption. For semiconductors with more complex defect states, such as CdSe in our study (and probably all earlier reports on CdSe as well as some reports for CdSeTe^[12,13,34–36]), radiative emission can be strong, but carrier mobility can be low, making it necessary to apply device models – not thermodynamics alone – for understanding device performance.^[12,13,37] A similarly complex relationship between radiative emission and device performance was suggested for CdSeTe solar cells^[38] and for some perovskite solar cells.^[39] In such “realistic” cases for absorbers that are not yet “ideal”, thermodynamics only partially indicates what can be realized at the current stage of material and device development. As a next step after absorption/emission analysis, we consider characteristics that define charge carrier transport: carrier lifetime τ_{SRH} , mobility μ , and diffusion length L_d , which are critical parameters for understanding performance when carrier traps are present.

In Figure 6 we compare carrier lifetimes in CdSe_xTe_{1-x} using references listed in the legend and include V_{OC} for absorbers that were completed to devices. Glockler, Sankin, and Zhao summarized data for CdTe ($x = 0$) solar cells with $V_{OC} = 840$ – 903 mV and TRPL lifetimes $\tau_{TRPL} = 2$ – 30 ns.^[41] For CdSe ($x = 1$) τ_{TRPL} were reported by Li et al.,^[4] Xue et al.,^[7] and in this study. For intermediate x compositions τ_{TRPL} increased up to 1200 ns^[42,43] due to grain boundary (GB) and extended defect passivation in the bulk^[44] and surface recombination velocity reduction to $S \approx 100$ cm s⁻¹ for CdSe_{0.2}Te_{0.8}/Al₂O₃ interfaces.^[45] As reported by Ablekim et al., τ_{TRPL} reached 250 ns in CdSe_{0.3}Te_{0.7} without surface passivation with Al₂O₃.^[46]

In the CdTe solar cell literature, it was long assumed that increasing carrier lifetime is the most promising pathway to higher

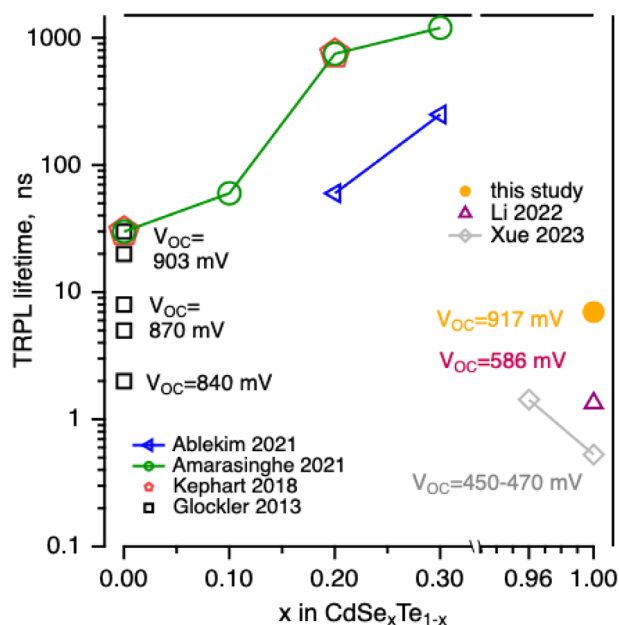


Figure 6. Minority carrier lifetimes in polycrystalline CdSe_xTe_{1-x} (CdTe at far left and CdSe at far right). For $x = 0$ and $x = 1$, device V_{OC} are also given in the figure. The best-reported V_{OC} for CdSe_xTe_{1-x} (in a graded bandgap device with $x \approx 0.25$ near the front junction) was 917 mV.^[40]

voltage.^[47,38] Data Figure 6 strongly suggests that V_{OC} is also contingent on other factors. E.g., voltages are comparable for $x = 0$ (903 mV),^[38] $x \approx 0.25$ (917 mV in a device with a graded bandgap with this composition near the front interface),^[44] and $x = 1$ (917 mV, this study), where recombination lifetimes differ by more than an order of magnitude. Changes in bandgap and free carrier density (doping) have rather minimal effect on the voltage/lifetime/composition trends in Figure 6. For example, increase in bandgap between $x = 0$ ($E_g = 1.5$ eV) to $x = 1$ ($E_g = 1.7$ eV) and increase in free carrier density by $\approx 100\times$ for the same samples results in V_{OC} gain of only + (15–50) mV.

We suggest that carrier trapping by defects D1 and D2 identified in Sections 2.2–2.4 is a key limitation for CdSe. As a result, better performance is obtained for thin absorbers. (In contrast, spectroscopy for CdTe devices with $V_{OC} \approx 900$ mV did not identify trapping effects^[48,49]). Trapping can negatively affect solar cells by reducing mobility.^[12,13,36,37] A density of traps N_t at energy E_a from the band edge (with $E_a \gg k_B T$) results in reduced mobility μ_{trap} .^[50]

$$\mu_{trap} = \mu_h \left[1 + \frac{N_t}{N_v} \exp\left(\frac{E_a}{k_B T}\right) \right]^{-1} \quad (3)$$

where μ_h is mobility without trapping and N_v is the effective density of states at the band edge. Using N_t and E_a found in this study, Equation (3) predicts ≈ 30 times lower μ_{trap} in comparison to μ_h . Hill et al. found electron Hall mobilities $\mu_e = 10$ – 100 cm² V⁻¹ s⁻¹ in our polycrystalline absorbers.^[6] Since hole effective mass is ≈ 3.5 times higher, the estimated free hole mobility is $\mu_h = 3$ – 30 cm² V⁻¹ s⁻¹, whereas due to trapping, the mobility is reduced to $\mu_{trap} = 0.1$ – 1 cm² V⁻¹ s⁻¹.

Minority carrier diffusion length is

$$L_d = \sqrt{D_h \tau_{SRH}} \quad (4)$$

where diffusivity

$$D_h = \frac{k_B T}{e} \mu_h \quad (5)$$

Therefore, due to trapping diffusion length decreases from

$$L_d = 0.2 - 0.7 \mu\text{m} \quad (\tau_{SRH} = 7 \text{ ns}, \mu_h = 3 - 30 \text{ cm}^2\text{V}^{-1}\text{s}^{-1})$$

$$\text{to } L_{d,\text{trapping}} = 0.05 - 0.15 \mu\text{m}$$

$$(\tau_{SRH} = 7 \text{ ns}, \mu_{\text{trap}} = 0.1 - 1 \text{ cm}^2\text{V}^{-1}\text{s}^{-1}) \quad (6)$$

which appears to be a critical limitation for CdSe solar cells. As a result, better performance is obtained with thin CdSe absorbers, when their thickness (0.5 μm) approaches $L_{d,\text{trapping}}$.

3. Summary and Conclusion

We reported improved CdSe solar cell performance where V_{OC} increased more than +300 mV from the literature study^[4] and +165 mV from our initial report.^[6] This improvement was achieved by using thin absorbers. Reduction of trap density ($N_t = (5-50) \times 10^{17} \text{ cm}^{-3}$ in this study) needs to be a future focus, because traps D1/D2 are not expected to be saturated at 1 Sun. Using detrapping lifetime $k_2^{-1} = 1 \mu\text{s}$, the estimated photogenerated minority carrier density is $\approx 10^{15} \text{ cm}^{-3}$, at least 10–100 times less than N_t . Thus, to improve device performance, reduction of trap density at least 10–100 times is required. Since DFT calculations indicate that D1 properties are consistent with the expected optoelectronic behavior of Se vacancies and D2 has been attributed to O on the group VI site, post-deposition selenization^[51] and tellurization^[7] are potential avenues for trap mitigation. Since CdSe absorbers are highly crystalline (exhibit exciton PL at low temperature and have E_u values comparable to those in single crystals), a reduction in trapping can in principle significantly improve transport characteristics potentially increasing mobility to single-crystal values.^[52] Reducing SRH recombination is also important: minority carrier lifetime was $\tau_{SRH} = 7 \text{ ns}$ in our samples, about two orders of magnitude lower than the radiative lifetime limit (radiative lifetime $\tau_R = 1/(Bn) \approx 500 \text{ ns}$, where radiative constant $B = 2 \times 10^{-10} \text{ cm}^3\text{s}^{-1}$ and $n \approx 10^{16} \text{ cm}^{-3}$).^[6] When τ_{SRH} reaches the radiative limit, PLQY would also increase by about two orders of magnitude, to PLQY $\approx 10^{-2}$, the value typical for the best polycrystalline absorbers.^[27]

We showed that polycrystalline CdSe have D1 and D2 defect states similar to those in CdSe single crystals,^[22–24] attributing defects to semiconductor bulk (not interfaces such as grain boundaries). Defect D1/D2 emission spectra in this study and in earlier reports^[23,24] are very similar to PL spectra for CdSe_xTe_{1-x},^[12,13,32–34] suggesting that mobility-limiting defects in binary CdSe and ternary CdSe_xTe_{1-x} absorbers may have similar characteristics. Since hole traps in CdSe and CdSe_xTe_{1-x}^[12,13] have similar characteristics, improvements in one material may inform advances for the other. The carrier trap assignment is supported by density functional theory calculations.

In contrast, band tails are much smaller in CdSe (this study) than CdSeTe.^[12,13,32–35] In polycrystalline absorbers band tails are commonly attributed to bandgap^[53] and electrostatic potential fluctuations.^[54] For example, high density of compensating defects can create electrostatic potential fluctuations, which was shown for group-V doped Cd(Se)Te.^[55] Such characteristics are not observed for CdSe. While CdSe has sufficient carrier density for efficient solar cells ($n = 10^{16} \text{ cm}^{-3}$),^[6] it has near-single-crystal band edge emission. This aspect is very useful for potential tandem applications, as band tails in the top junction absorber can complicate light absorption by the bottom junction, photon management, and junction photon coupling.^[2]

4. Experimental Section

Solar Cell Fabrication and Characterization: CdSe absorbers were deposited on commercial soda-lime glass coated with fluorine-doped tin oxide (FTO) using vapor-transport deposition (VTD).^[6] The as-deposited CdSe films are intrinsically *n*-type^[56] and polycrystalline with grains in the nanometer range. Optoelectronic properties of as-deposited CdSe were improved with a CdCl₂ heat treatment (CHT)^[57–59] applied by spin-coating aqueous CdCl₂ onto CdSe surface and annealing at 400–500 °C for 20–60 min. in a mixture of nitrogen and oxygen at 500 torr. CHT promotes large grain growth, to >5 μm on average, improves external radiative efficiency by orders-of-magnitude, and increases charge carrier lifetimes from the picosecond to the nanosecond range.^[6] PL emission spectra prior and after CHT treatment indicate ≈ 100 times increased radiative efficiency and some decrease in band tails.^[6,14] Columnar grain structure in CdSe films is shown in cross-sectional SEM images (Figure S6, Supporting Information).^[14]

Device stack optimization, and specifically the development of the transparent hole-contact stack (PTAA/MoO₃/Au), was also described previously.^[6] In addition, the properties of the PTAA (poly(triaryl) amine) hole transport layer (HTL) have been reported by Hack et al,^[60] and the PTAA HTL impact on interface recombination has been characterized.^[61] Optimized PTAA concentration in solution was 10 mg mL⁻¹ (PTAA layer thickness 10–50 nm), MoO₃ thickness was 5 nm, and gold layer thickness was 10 nm.^[14] The development of transparent hole contacts allows solar-cell use in the substrate geometry (Figure 1a) and is essential for potential future applications as a top junction in a tandem solar cell architecture. Previously reported Hall measurements identified *n*-type conductivity with $n \approx 10^{16} \text{ cm}^{-3}$ and electron mobility $\mu_n = 10-100 \text{ cm}^2 \text{ V}^{-1} \text{ s}^{-1}$.⁶ The carrier concentration was also confirmed by capacitance-voltage (CV) measurements on devices.^[6]

Spectroscopy: PL emission spectra were measured with spectrally corrected Si CCD and InGaAs linear array detectors (Pixis F100 and PyLoN-1024 IR, Princeton Instruments) using an $f = 300 \text{ mm}$ spectrograph. Calibration with absolute photon numbers was performed using 2% reflectance standards (Lab Sphere). The excitation wavelength was 442 nm (He-Cd laser) for the variable-temperature PL measurements and 632.8 nm (He-Ne laser) for the absolute PL measurements. For TRPL excitation at 450 nm, a Pharos/Orpheus KGW:Yb optical parametric amplifier laser system was used (Light Conversion, 300 fs pulses at 1.1 MHz and lower repetition rates). Time-correlated single photon counting (with PicoHarp 300 electronics, Picoquant) and detection with Si and gated InGaAs/InP avalanche photodiodes (both from Micro Photon Devices) was used. Closed loop He cryostats were used for low temperature PL and TRPL measurements.

Density Functional Theory Calculations: DFT calculations were performed with the Vienna ab initio simulation package (VASP),^[62] in which the ion-cores are described by the projected augmented wave (PAW) method.^[63] Perdew–Burke–Ernzerhof exchange–correlation functional^[64] was employed with the spin polarization included in both the electronic calculations and the structural relaxation of bulk cells and supercells with defects. The kinetic energy cutoff for plane-wave basis was set to 520 eV,

and the convergence criteria for electronic self-consistent loops and ion relaxation loops are 10^{-5} eV and 5 meV/angstrom, respectively. Effective Hubbard parameters^[65] in the simplified (rotationally invariant) approach were employed on d orbitals of Cd ($U_{\text{eff}} = 12$ eV), which gives bandgap value and lattice parameters comparable to experimental results for both CdSe and CdTe.^[26] The supercell for defect calculations consists of 300 atoms and the k-point sampling contained a single- Γ point. Charged-cell correction to defect formation energies (DFE) due to the interaction of localized defect charge in a finite-size supercell with its periodic images was calculated in the Freysoldt, Neugebauer, and Van de Walle (FNV) correction scheme.^[66] Configuration coordinate diagrams (CCD) were calculated according to linearly interpolated structures between two fixed ground state structures belonging to two different defect charge states.

Supporting Information

Supporting Information is available from the Wiley Online Library or from the author.

Acknowledgements

This work was authored in part by the National Renewable Energy Laboratory for the U.S. Department of Energy (DOE) under Contract No. DE-AC36-08GO28308. Funding provided by the U.S. Department of Energy's Office of Energy Efficiency and Renewable Energy (EERE) under the Solar Energy Technology Office (SETO) Award Nos. 38525, DE-EE0008974, DE-EE0008556, and 52778. Further support was provided under NSF MRSEC DMR-2308979. The computational work was facilitated through the use of the Hyak supercomputer system at the University of Washington (UW) provided via the MEM-C MRSEC and the UW Clean Energy Institute and Student Technology Fund. The views expressed in the article do not necessarily represent the views of the DOE or the U.S. Government. The U.S. Government retains and the publisher, by accepting the article for publication, acknowledges that the U.S. Government retains a nonexclusive, paid-up, irrevocable, worldwide license to publish or reproduce the published form of this work, or allow others to do so, for U.S. Government purposes.

Conflict of Interest

The authors declare no conflict of interest.

Data Availability Statement

The data that support the findings of this study are available in the supplementary material of this article.

Keywords

CdSe solar cells, charge carrier trapping, density functional theory, Se vacancies, thin film photovoltaics

Received: September 24, 2025
Published online:

- [1] <https://www.nrel.gov/pv/cell-efficiency.html>, (accessed: August 2025).
[2] K. Alberi, J. J. Berry, J. J. Cordell, D. J. Friedman, J. F. Geisz, A. R. Kirmani, B. W. Larson, W. E. McMahon, L. M. Mansfield, P. F. Ndione, M. Owen-Bellini, A. F. Palmstrom, M. O. Reese, S. B. Reese, M. A. Steiner, A. C. Tamboli, S. Theingi, E. L. Warren, *Joule* **2024**, *8*, 658.

- [3] J. Y. Ye, R. A. Kerner, Q. Jiang, F. Yang, J. Yang, M. Ahmadi, S. P. Harvey, K. X. Steirer, D. Kuciauskas, J. J. Berry, K. Zhu, *InfoMat* **2024**, *7*, 12643.
[4] K. Li, X. Yang, Y. Lu, J. Xue, S. Lu, J. Zheng, C. Chen, J. Tang, *Adv. Energy Mater.* **2022**, *12*, 2200725.
[5] E. Bastola, A. B. Phillips, A. Abudulium, V. Kornienko, Z. Hussain, M. K. Jamarkattel, T. Mariam, P. N. Kalurachchi, J. Friedl, D. Pokhrel, K. B. Kile, Z. Song, Y. Yan, M. Walls, R. J. Ellingson, M. J. Heben, In 2023 IEEE 50th Photovoltaic Specialists Conference (PVSC), IEEE, San Juan, PR, USA, **2023**, pp. 1–6.
[6] T. Hill, S. Grover, J. Sites, In 2023 IEEE 50th Photovoltaic Specialists Conference (PVSC), IEEE, NY, **2023**, pp. 1–6.
[7] J. Xue, X. Yang, X. Bao, L. Fu, S. Li, M. Huang, J. Wang, H. Song, S. Chen, C. Chen, K. Li, J. Tang, *ACS Appl. Mater. Interfaces* **2023**, *15*, 17858.
[8] X. Bao, J. Xue, X. Yang, J. Liu, H. Yang, Z. Tang, J. Tang, C. Chen, X. Zeng, K. Li, *Sol. Energy Mater. Sol. Cells* **2024**, *272*, 112878.
[9] A. R. Duggal, J. J. Shiang, W. Hullinger, H. A. F. Halverson, US Patent US20140373908, **2014**, <https://patents.google.com/patent/US20140373908A1/en>.
[10] N. Rosenblatt, J. Hack, C. Lee, Y.-H. Zhang, W. K. Metzger, *APL Mater.* **2024**, *12*, 111117.
[11] I. Khatir, C. Kasik, J. R. Sites, *IEEE J. Photovoltaics* **2024**, *14*, 745.
[12] P. Ščajev, M. Nardone, C. Reich, R. Farshchi, K. McReynolds, D. Krasikov, D. Kuciauskas, *Adv. Energy Mater.* **2025**, *15*, 2403902.
[13] D. Kuciauskas, M. Nardone, A. Bothwell, D. Albin, C. Reich, C. Lee, E. Colegrove, *Adv. Energy Mater.* **2023**, *13*, 2301784.
[14] T. Hill, Ph.D. Thesis, Colorado State University **2025**, <https://mountainscholar.org/items/75987311-0a10-430e-8b5d-843e6f53c4e4>.
[15] M. A. Green, A. W. Y. Ho-Baillie, *ACS Energy Lett.* **2019**, *4*, 1639.
[16] D. Kuciauskas, J. Moseley, C. Lee, *Solar RRL* **2021**, *5*, 2000775.
[17] D. Kuciauskas, J. Moseley, P. Ščajev, D. Albin, *Phys. Status Solidi RRL* **2020**, *14*, 1900606.
[18] L. Krückemeier, U. Rau, M. Stalterfoht, T. Kirchartz, *Adv. Energy Mater.* **2020**, *10*, 1902573.
[19] J. Jean, T. S. Mahony, D. Bozyigit, M. Sponseller, J. Holovský, M. G. Bawendi, V. Bulović, *ACS. Energy Lett.* **2017**, *2*, 2616.
[20] M. H. Wolter, R. Carron, E. Avancini, B. Bissig, T. P. Weiss, S. Nishiwaki, T. Feurer, S. Buecheler, P. Jackson, W. Witte, S. Siebentritt, *Prog. Photovoltaics* **2022**, *30*, 702.
[21] Y. Kokubun, H. Watanabe, M. Wada, *Jpn. J. Appl. Phys.* **1974**, *13*, 1393.
[22] C. H. Chia, C. T. Yuan, J. T. Ku, S. L. Yang, W. C. Chou, J. Y. Juang, S. Y. Hsieh, K. C. Chiu, J. S. Hsu, S. Y. Jeng, *J. Lumin.* **2008**, *128*, 123.
[23] L. Kindleysides, J. Woods, *J. Phys. D: Appl. Phys.* **1970**, *3*, 1049.
[24] I. B. Ermolovich, V. V. Milenin, *Physica Status Solidi*. **1986**, *133*, 611.
[25] M. J. S. Brasil, P. Motisuke, F. Decker, J. R. Moro, *J. Phys. C: Solid State Phys.* **1988**, *21*, 3141.
[26] Z. Ju, X. Qi, S. Schaefer, M. R. McCartney, D. J. Smith, A. V. G. Chizmeshya, T. McCarthy, A. McMinn, S. Grover, Y.-H. Zhang, *IEEE J. Photovoltaics* **2024**, *14*, 752.
[27] X. Xiang, Y. Tong, A. Gehrke, S. T. Dunham, *Phys. Rev. Mater.* **2024**, *8*, 084602.
[28] M. Stalterfoht, C. M. Wolff, J. A. Márquez, S. Zhang, C. J. Hages, D. Rothhardt, S. Albrecht, P. L. Burn, P. Meredith, T. Unold, D. Neher, *Nat. Energy* **2018**, *3*, 847.
[29] D. Kuciauskas, M. Nardone, P. Ščajev, C.-S. Jjiang, D. Lu, R. Farshchi, N. Comm, *Nat. Commun.* **2025**, *16*, 8378.
[30] S. Rühle, *Sol. Energy* **2016**, *130*, 139.
[31] J. Wong, S. T. Omelchenko, H. A. Atwater, *ACS Energy Lett.* **2021**, *6*, 52.
[32] T. Unold, L. Gütay, In *Advanced Characterization Techniques for Thin Film Solar Cells*, 2nd ed.; (Eds.: D. Abou-Ras, T. Kirchartz, U. Rau), Wiley-VCH, Weinheim, **2016**, Ch.1.
[33] T. Kirchartz, U. Rau, *Adv. Energy Mater.* **2018**, *8*, 1703385.

- [34] P. Jundt, R. Arndt, C. Drost, S. Baitule, B. Späth, B. Siepchen, O. Zywitzki, T. Modes, In 2024 IEEE 52nd Photovoltaic Specialist Conference (PVSC) IEEE, Seattle, WA, USA **2024**, pp. 692.
- [35] S. Myneni, D. Shaw, A. Munshi, W. Sampath, In 2024 IEEE 52nd Photovoltaic Specialist Conference (PVSC) IEEE, Seattle, WA, USA **2024**, pp. 0887.
- [36] D. L. McGott, S. W. Johnston, C. Jiang, T. Liu, D. Kuciauskas, S. Glynn, M. O. Reese, *Adv. Sci.* **2024**, *11*, 2309264.
- [37] M. Nardone, S. Gupta, E. Mulloy, S. Johnston, E. Colegrove, J. N. Duenow, B. Good, C. L. Perkins, D. Kuciauskas, M. O. Reese, *Phys. Rev. Applied* **2025**, *23*, 034019.
- [38] D. Krasikov, D. Kuciauskas, P. Ščajev, R. Farshchi, K. McReynolds, I. Sankin, *Prog. in Photovoltaics* **2025**,
- [39] J. Warby, S. Shah, J. Thiesbrummel, E. Gutierrez-Partida, H. Lai, B. Alebachew, M. Grischek, F. Yang, F. Lang, S. Albrecht, F. Fu, D. Neher, M. Stolterfoht, *Adv. Energy Mater.* **2023**, *13*, 2303135.
- [40] R. Mallick, X. Li, C. Reich, X. Shan, W. Zhang, T. Nagle, L. Bok, E. Bicakci, N. Rosenblatt, D. Modi, R. Farshchi, C. Lee, J. Hack, S. Grover, N. Wolf, W. K. Metzger, D. Lu, G. Xiong, *IEEE J. Photovoltaics* **2023**, *13*, 510.
- [41] M. Gloeckler, I. Sankin, Z. Zhao, *IEEE J. Photovoltaics* **2013**, *3*, 1389.
- [42] J. M. Kephart, A. Kindvall, D. Williams, D. Kuciauskas, P. Dippo, A. Munshi, W. S. Sampath, *IEEE J. Photovoltaics* **2018**, *8*, 587.
- [43] M. Amarasinghe, D. Albin, D. Kuciauskas, J. Moseley, C. L. Perkins, W. K. Metzger, *Appl. Phys. Lett.* **2021**, *118*, 211102.
- [44] T. A. M. Fiducia, B. G. Mendis, K. Li, C. R. M. Grovenor, A. H. Munshi, K. Barth, W. S. Sampath, L. D. Wright, A. Abbas, J. W. Bowers, J. M. Walls, *Nat. Energy* **2019**, *4*, 504.
- [45] D. Kuciauskas, J. M. Kephart, J. Moseley, W. K. Metzger, W. S. Sampath, P. Dippo, *Appl. Phys. Lett.* **2018**, *112*, 263901.
- [46] T. Ablekim, J. N. Duenow, C. L. Perkins, J. Moseley, X. Zheng, T. Bidaud, B. Frouin, S. Collin, M. O. Reese, M. Amarasinghe, E. Colegrove, S. Johnston, W. K. Metzger, *Solar RRL* **2021**, *5*, 2100173.
- [47] W. K. Metzger, D. Albin, D. Levi, P. Sheldon, X. Li, B. M. Keyes, R. K. Ahrenkiel, *J. Appl. Phys.* **2003**, *94*, 3549.
- [48] D. Kuciauskas, P. Dippo, Z. Zhao, L. Cheng, A. Kanevce, W. K. Metzger, M. Gloeckler, *IEEE J. Photovoltaics* **2016**, *6*, 313.
- [49] D. Kuciauskas, P. Dippo, A. Kanevce, Z. Zhao, L. Cheng, A. Los, M. Gloeckler, W. K. Metzger, *Appl. Phys. Lett.* **2015**, *107*, 243906.
- [50] N. F. Mott, E. A. Davis, *Electronic processes in non-crystalline materials*, Oxford University Press, Oxford, **2012**.
- [51] B. Bagheri, R. Kottokaran, L.-P. Poly, B. Reichert, S. Sharikadze, M. Noack, V. Dalal, *AIP. Adv.* **2019**, *9*, 125012.
- [52] M. Murugesan, S. Swain, J. McCloy, In 2024 IEEE 52nd Photovoltaic Specialist Conference (PVSC), IEEE, Seattle, WA, USA, **2024**, pp. 1166–1168.
- [53] U. Rau, J. H. Werner, *Appl. Phys. Lett.* **2004**, *84*, 3735.
- [54] B. I. Shklovskii, A. L. Efros, *Springer Sci. Business Media*, Springer-Verlag, Berlin Heidelberg **2013**, 45.
- [55] J. Moseley, S. Grover, D. Lu, G. Xiong, H. L. Guthrey, M. M. Al-Jassim, W. K. Metzger, *J. Appl. Phys.* **2020**, *128*, 103105.
- [56] H. Berger, G. Jäniche, N. Grachovskaya, *Physica Status Solidi* **1969**, *33*, 417.
- [57] S. L. Patel, S. C. Himanshu, A. Purohit, M. D. Kannan, M. S. Dhaka, *Optical Mater.* **2019**, *89*, 42.
- [58] S. L. Patel, K. Himanshu, S. Chander, M. D. Kannan, M. S. Dhaka, *J. Mater. Sci.: Mater. Electron.* **2019**, *30*, 20840.
- [59] R. C. Greenhalgh, V. Kornienko, M. Togay, A. Abbas, E. Bastola, A. B. Phillips, M. J. Heben, J. Bowers, J. M. Walls, In 2023 IEEE 50th Photovoltaic Specialists Conference (PVSC), IEEE, San Juan, PR, USA, **2023**, pp. 1–4.
- [60] J. Hack, C. Lee, S. Grover, G. Xiong, In 2021 IEEE 48th Photovoltaic Specialists Conference (PVSC), IEEE, Fort Lauderdale, FL, USA, **2021**, pp. 1880–1882.
- [61] D. Kuciauskas, C. L. Perkins, M. Nardone, C. Lee, R. Mallick, G. Xiong, *Solar RRL* **2023**, *7*, 2300073.
- [62] G. Kresse, J. Furthmüller, *Comput. Mater. Sci.* **1996**, *6*, 15.
- [63] G. Kresse, D. Joubert, *Phys. Rev. B* **1999**, *59*, 1758.
- [64] J. P. Perdew, A. Ruzsinszky, G. I. Csonka, O. A. Vydrov, G. E. Scuseria, L. A. Constantin, X. Zhou, K. Burke, *Phys. Rev. Lett.* **2008**, *100*, 136406.
- [65] S. L. Dudarev, G. A. Botton, S. Y. Savrasov, C. Humphreys, A. P. Sutton, *Phys. Rev. B* **1998**, *57*, 1505.
- [66] C. Freysoldt, J. Neugebauer, C. G. Van de Walle, *Physica Status Solidi* **2011**, *248*, 1067.